Biochemistry

Article

Cite This: Biochemistry 2019, 58, 4570−4581

pubs.acs.org/biochemistry

The Solution Structure and Dynamics of Cd-Metallothionein from *Helix pomatia* Reveal Optimization for Binding Cd over Zn

Andrea Beil,[†] Simon Jurt,[†] Reto Walser,[†,@] Tanja Schönhut,[†] Peter Güntert,[‡,§] Òscar Palacios,[∥] Silvia Atrian,[⊥,∇] Mercè Capdevila,[∥] Reinhard Dallinger,[*,#] and Oliver Zerbe[*,†]

[†]Department of Chemistry, University of Zurich, Winterthurerstrasse 190, CH-8057 Zürich, Switzerland

[‡]Institute of Biophysical Chemistry, Goethe-University Frankfurt am Main, Max-von-Laue-Strasse 9, 60438 Frankfurt am Main, Germany

[§]Laboratory of Physical Chemistry, ETH Zürich, 8093 Zürich, Switzerland

[∥]Departmento de Química, Facultat de Ciències, Universitat Autònoma de Barcelona, E-08193 Cerdanyola del Vallès, Barcelona, Spain

[⊥]Departmento de Genètica, Facultat de Biologia, Universitat de Barcelona, Av. Diagonal 645, E-08028 Barcelona, Spain

[#]Institute of Zoology and Center of Molecular Biosciences Innsbruck (CMBI), University of Innsbruck, Technikerstraße 25, A-6020 Innsbruck, Austria

Supporting Information

Downloaded via ETH ZURICH on November 14, 2019 at 09:01:01 (UTC).
See https://pubs.acs.org/sharingguidelines for options on how to legitimately share published articles.

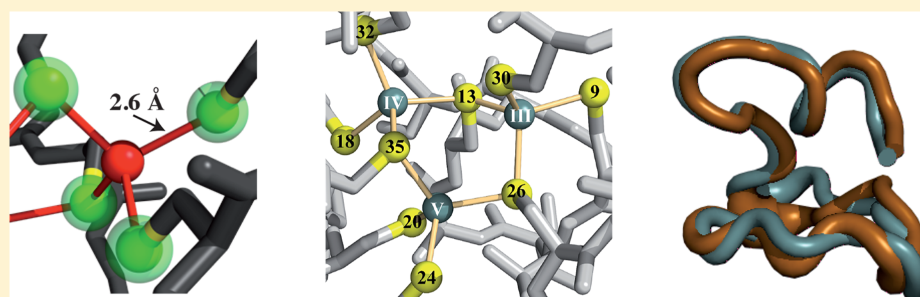

ABSTRACT: Metallothioneins (MTs) are cysteine-rich polypeptides that are naturally found coordinated to monovalent and/or divalent transition metal ions. Three metallothionein isoforms from the Roman snail *Helix pomatia* are known. They differ in their physiological metal load and in their specificity for transition metal ions such as Cd^{2+} (HpCdMT isoform) and Cu^{+} (HpCuMT isoform) or in the absence of a defined metal specificity (HpCd/CuMT isoform). We have determined the solution structure of the Cd-specific isoform (HpCdMT) by nuclear magnetic resonance spectroscopy using recombinant isotopically labeled protein loaded with Zn^{2+} or Cd^{2+}. Both structures display two-domain architectures, where each domain comprises a characteristic three-metal cluster similar to that observed in the β-domains of vertebrate MTs. The polypeptide backbone is well-structured over the entire sequence, including the interdomain linker. Interestingly, the two domains display mutual contacts, as observed before for the metallothionein of the snail *Littorina littorea*, to which both N- and C-terminal domains are highly similar. Increasing the length of the linker motionally decouples both domains and removes mutual contacts between them without having a strong effect on the stability of the individual domains. The structures of Cd_6- and Zn_6-HpCdMT are nearly identical. However, ^{15}N relaxation, in particular ^{15}N R_2 rates, is accelerated for many residues of Zn_6-HpCdMT but not for Cd_6-HpCdMT, revealing the presence of conformational exchange effects. We suggest that this snail MT isoform is evolutionarily optimized for binding Cd rather than Zn.

Members of the protein superfamily of metallothioneins (MTs) are characterized by chemical, structural, and functional features related to the ability of these proteins to bind d^{10} metals such as Zn^{2+}, Cd^{2+}, and Cu^{+} with high affinity.[1] The metal ions are coordinated by the sulfur atoms of the protein's cysteine residues and, in fewer cases, by nitrogen atoms from His residues.[2] Thereby, they form characteristic metal clusters in which some of the thiolate ligands are shared in a bridging manner by two metal ions, conferring the polypeptide chain a well-defined conformation.[3] All three-dimensional (3D) structures of animal MTs known until recently reveal dumbbell shapes comprising two spatially well-defined globular domains, each of them housing one divalent metal thiolate cluster,[4,5] separated from each other by a linker of two to four residues. Owing to the flexibility of this linker, the mutual orientation of the two domains has often remained

Received: September 10, 2019
Revised: October 11, 2019
Published: October 21, 2019

ACS Publications © 2019 American Chemical Society

poorly defined during structure determination by nuclear magnetic resonance (NMR)[6] and has been largely precluded analysis by crystallography.

Among all MT structures known so far, only four are from invertebrate animals, those of sea urchin (*Strongylocentrotus purpuratus*),[6] blue crab (*Callinectes sapidus*),[7] lobster (*Homarus americanus*),[8] and the marine snail *Littorina littorea*.[9] Interestingly, the *L. littorea* metallothionein (LlMT) comprises three domains, each presenting a three-metal cluster, thereby conferring upon this MT the capability to bind an increased amount of toxic Cd^{2+} metal ions. The 3D structures of these invertebrate Cd-MT complexes differ in many details that are expected to deeply affect their functionality. So far, it has been impossible to predict the 3D structure of MTs from their amino acid sequence,[5] even if the bound metal ion is known. The limited knowledge of MT structures is in striking contrast to the vast number of primary sequences available from invertebrates of very different taxa, spanning a broad range of protein lengths, amino acid compositions, and numbers and distributions of amino acid motifs supposed to be involved in metal binding.[10,11] Moreover, there is a growing body of evidence that shows that peculiar functions among invertebrate MTs may vary in a taxon- or species-specific manner, or even among different isoforms within a given species.[12,13]

A particularly diverse and interesting subfamily of MTs is that of pulmonate snails. These organisms belong to the phylum Mollusca and have evolved, in contrast to many other species, metal-specific MT isoforms. Hence, they possess MTs, which can be isolated from preparations *in vivo* after exposure of the snails to these metal ions as nearly pure, homometallic metal complexes, loaded exclusively with either Cu^{+} or Cd^{2+}.[14] For example, terrestrial pulmonates such as the Roman snail (*Helix pomatia*) express, on one hand, a Cu-specific MT isoform (HpCuMT) in a particular cell type called rhogocytes.[15,16] These serve Cu-homeostatic functions in connection with hemocyanin synthesis.[17] On the other hand, a second, Cd-specific MT isoform (HpCdMT) is expressed in the snail digestive and excretory tissues and binds nearly exclusively and with high affinity Cd^{2+} ions, thus shielding the snail organism efficiently against environmental concentrations of this toxic metal.[16,18] In the absence of Cd^{2+}, this isoform appears to be present at only low basal concentrations in association with Zn^{2+} ions, for which it probably plays also a homeostatic role.[19] Metal specificity in this case refers to the couple of the two transition metal ions Cd^{2+} and Zn^{2+}. Consequently, molecular evolution of MTs in pulmonate snails has led to a complete separation of metal-related functional tasks,[20] a feature that is related to differences in sequence and most likely also three-dimensional structure.

The two metal-specific MT isoforms of *H. pomatia* also exhibit their specific metal binding behavior when recombinantly synthesized in metal-supplemented *Escherichia coli* cells, as shown by isolation and analysis of the homometallic complexes of the two recombinant isoforms with their cognate metal ions.[20] Intriguingly, the two isoforms (HpCdMT and HpCuMT) have achieved metal specificity by evolutionary optimization of primary structure, and this must have been achieved through residues that do not directly coordinate the metals but rather influence the 3D structure of the protein.[20] To understand how these proteins can distinguish between their cognate and noncognate metal ions and how the non-cysteine amino acid residues contribute to this specificity, we determined the 3D solution structure of the Cd-specific HpCdMT isoform and its Zn-loaded variant.

In this work, we demonstrate that high-quality structures of both the Zn and Cd species can be determined owing to novel approaches using NMR data from ^{13}C- and ^{15}N-labeled proteins. We compare our structures of HpCdMT to published structures from invertebrates and other known species. We particularly focus in our analysis on correlations between evolutionary distances of species and the similarity in their 3D structure and the topology of the three-metal clusters.

■ METHODS

Chemicals and Materials. [^{13}C]Glucose, $^{15}NH_4Cl$, and perdeuterated Tris buffer were purchased from Spectra Stable Isotopes. $^{113}CdCl_2$ was obtained as a kind gift from M. Vašák. Glutathione sepharose 4B and thrombin were bought from GE Healthcare. TCEP was purchased from Hampton Research, and isopropyl *β*-D-1-thiogalactopyranoside from Biosolve. All other standard biochemical grade chemicals were ordered from Sigma.

Size exclusion chromatography (SEC) steps were carried out on a GE Healthcare HiLoad 16/60 Superdex 75pg column. Solutions were always freshly purged with argon.

Recombinant Expression and Purification of HpCdMT and HpMcCdMT. The HpCdMT isoform of *H. pomatia* metallothionein (HpCdMT) and its mutant HpMcCdMT were expressed in *E. coli* BL21 (DE3) as described previously.[20−22] Higher yields of the Cd-loaded variant prompted us to express the Cd-loaded species and produce the Zn-containing form via a subsequent metal exchange. The details concerning the cloning and plasmid topology are given in refs 20 and 23.

Metal Exchange. Metal exchange to replace $^{112}Cd^{2+}$ ions with NMR-active $^{113}Cd^{2+}$ and to convert the Cd_6 into the Zn_6 species was achieved by demetalation with a decrease in pH (pH 2) in a reducing milieu [10 mM tris(2-carboxyethyl)-phosphine (TCEP)], complete elimination of any free metal ions, and readjustment to neutral pH to yield the apo form, from which the differently metalated forms were obtained using the following procedure. First, 0.2 mL of a Cd-HpCdMT solution was diluted to 1 mL by adding argon-purged 20 mM Tris-HCl and 10 mM TCEP (pH 7) and transferred to a concentrating tube (Amicon Ultra-4 3K Centrifugal Filter Device, EMD Millipore). The pH was decreased in four centrifugal steps (3500 RCF) by adding each time 3−3.5 mL of the same buffer that was used in the previous step (pH 2) and spinning it down to 0.5−1 mL. Using the reverse procedure (four centrifugal steps), each time adding 3.5 mL of 20 mM Tris-HCl buffer (pH 7), the pH was readjusted while any free metal ions were effectively removed. Incubation with 1.3 equiv of the corresponding metal ions (from $^{113}CdCl_2$ and $ZnCl_2$) dissolved in 1 mL of buffer (pH 7) over a period of 15 min achieved complete remetalation. Excess metal ions were removed in additional centrifugation steps after dilution with 20 mM Tris-HCl and 10 mM TCEP (pH 7).

NMR Spectroscopy. All spectra were recorded on samples at a protein concentration of approximately 1.0 mM in 10 mM [^{2}H]Tris and 1 mM TCEP (pH 7.0) at 298 K on Bruker AV-600 or AV-700 spectrometers equipped with cryoprobes. Proton chemical shifts were referenced to the water signal. Nitrogen shifts were referenced indirectly to liquid NH_3.[24] Raw data were processed using Bruker Topspin software versions 2.0 and 2.1 and transferred to CARA[25] for further

DOI: 10.1021/acs.biochem.9b00830
Biochemistry 2019, 58, 4570−4581

Table 1. Summary of Structure Calculations

	Cd-HpCdMT, ambiguous[b]	Cd-HpCdMT,[a] unambiguous[c]	Zn-HpCdMT,[a] unambiguous[c]
Input Data for Structure Calculation			
no. of NOE distance restraints			
total	968	992	962
short-range ($\|i - j\| \leq 1$)	565	577	535
medium-range ($1 < \|i - j\| < 5$)	185	189	217
long-range ($\|i - j\| \geq 5$)	218	226	210
Structural Statistics			
20 conformers, consensus run			
CYANA (NOE assignment)			
CYANA target function value (Å^2)	0.35 ± 0.04	0.39 ± 0.03	0.50 ± 0.05
RMSD (Å) for backbone atoms (residues 9–65)	1.46 ± 0.55	0.71 ± 0.26	0.86 ± 0.27
RMSD (Å) for backbone atoms (residues 9–35)	0.63 ± 0.19	0.36 ± 0.11	0.51 ± 0.23
RMSD (Å) for backbone atoms (residues 38–65)	0.46 ± 0.08	0.38 ± 0.14	0.28 ± 0.14
RMSD (Å) for heavy atoms (residues 9–65)	1.76 ± 0.56	1.01 ± 0.25	1.17 ± 0.27
RMSD (Å) for heavy atoms (residues 9–35)	1.09 ± 0.20	0.75 ± 0.16	0.97 ± 0.24
RMSD (Å) for heavy atoms (residues 38–65)	0.84 ± 0.09	0.77 ± 0.14	0.62 ± 0.09
Xplor-NIH (water refinement)			
energy (kcal/mol)	−1400 ± 84	−1446 ± 95	−1261 ± 68
NOE violations (number, threshold of 0.5)	0.1 ± 0.3	0.0 ± 0.0	0.0 ± 0.0
RMSD (Å) for backbone atoms (residues 9–65)	1.49 ± 0.60	0.76 ± 0.23	0.95 ± 0.30
RMSD (Å) for backbone atoms (residues 9–35)	0.69 ± 0.16	0.46 ± 0.08	0.60 ± 0.17
RMSD (Å) for backbone atoms (residues 38–65)	0.50 ± 0.08	0.40 ± 0.10	0.34 ± 0.07
RMSD (Å) for heavy atoms (residues 9–65)	1.80 ± 0.60	1.09 ± 0.22	1.28 ± 0.28
RMSD (Å) for heavy atoms (residues 9–35)	1.16 ± 0.17	0.88 ± 0.06	1.06 ± 0.20
RMSD (Å) for heavy atoms (residues 38–65)	0.89 ± 0.09	0.82 ± 0.10	1.37 ± 0.29
PROCHECK Ramachandran plot analysis			
residues in most favored regions (%)	72.4	77.4	79.9
residues in additional allowed regions (%)	23.2	21.1	17.2
residues in generously allowed regions (%)	3.2	0.3	2.4
residues in disallowed regions (%)	1.2	1.2	0.6

[a]Deposited in the Protein Data Bank. [b]Using generic metal–metal and metal–Cys-S^γ distances. [c]Adding explicit metal–Cys-S^γ (extracted from ^{113}Cd–^{1}H correlation spectra or from consensus runs).

analysis. All two-dimensional (2D) experiments utilized TPPI-States[26,27] for quadrature detection in indirect proton dimensions and gradient-selected coherence selection (echo–antiecho)[28] in combination with sensitivity enhancement schemes[28,29] in all experiments that detect amide protons.

Resonance Assignment. Backbone assignment was achieved with the help of 3D CBCA(CO)NH[30] and HNCACB[31] spectra. Side chain assignment was accomplished using a combination of 16 ms mixing time (H)CCH- and H(C)CCH-TOCSY[32,33] as well as 120 ms ^{13}C-[34] and ^{15}N-resolved NOESY[35] experiments.

Cd-Cys coordination was established with the help of a ^{113}Cd–^{1}H HMQC-TOCSY experiment utilizing the ^3J coupling between Cd and the β-protons of cysteine residues.[36,37] The J coupling evolution time in the HMQC experiment was set to 12.5 ms, and the TOSCY mixing time to 60 ms. A ^{15}N-labeled protein loaded with ^{113}Cd was used for this experiment.

Structure Calculation. NOE assignment and structure calculations were performed with CYANA 3.98.[38,39] NOESY peaks were automatically picked in CcpNMR,[40] followed by a manual check to eliminate artifacts and to add additional low-intensity peaks. Unassigned, integrated peak lists and chemical shift lists served as input for automatic NOESY peak assignment using the noeassign macro of CYANA.[39]

For the Cd-loaded variant, a total of 614 ^{15}N and 1353 ^{13}C NOESY cross peaks and for the Zn-loaded form 818 ^{15}N and 1084 ^{13}C NOESY cross peaks were used to generate distance restraints (Table 1). The first round of structure calculations was performed solely on the basis of NOE-derived distance restraints. In further runs, ambiguous metal restraints were introduced consisting of lower distance bounds between the metal ions in each cluster (3.6 Å for Cd and 3.0 Å and Zn) and 0.1 Å upper distance bounds between cysteine S^γ and dummy ligand atoms of pseudoresidues. For that purpose, an extra CYANA library entry was created consisting of a metal center with four ligand pseudoatoms in a tetrahedral geometry with no van der Waals radius spaced by 2.6 or 2.4 Å from the Cd or Zn ions, respectively (Figure S1). The input for the final structure calculation of the Cd-loaded variant contained 992 NOE-derived upper distance limits, including 226 long-range restraints. For the Zn variant, 962 restraints were used, of which 210 were long-range restraints (Figure S2). We noticed that while the precision strongly improved upon incorporation of the ambiguous restraints, the overall fold remained the same (Figure S3). Interestingly, calculations based on ambiguous metal restraints yielded almost unique metal–ligand connectivities among the lowest-energy conformers, and these connectivities agreed with the correlations observed in the ^{113}Cd–^{1}H HMQC spectra of the Cd-loaded variant. However, the root-mean-square deviation (RMSD) in the bundle was unreasonably low, and hence, 20 consensus runs starting from different initial structures were performed.[41] While the same metal–Cys connectivities existed in these independent runs,

DOI: 10.1021/acs.biochem.9b00830
Biochemistry 2019, 58, 4570–4581

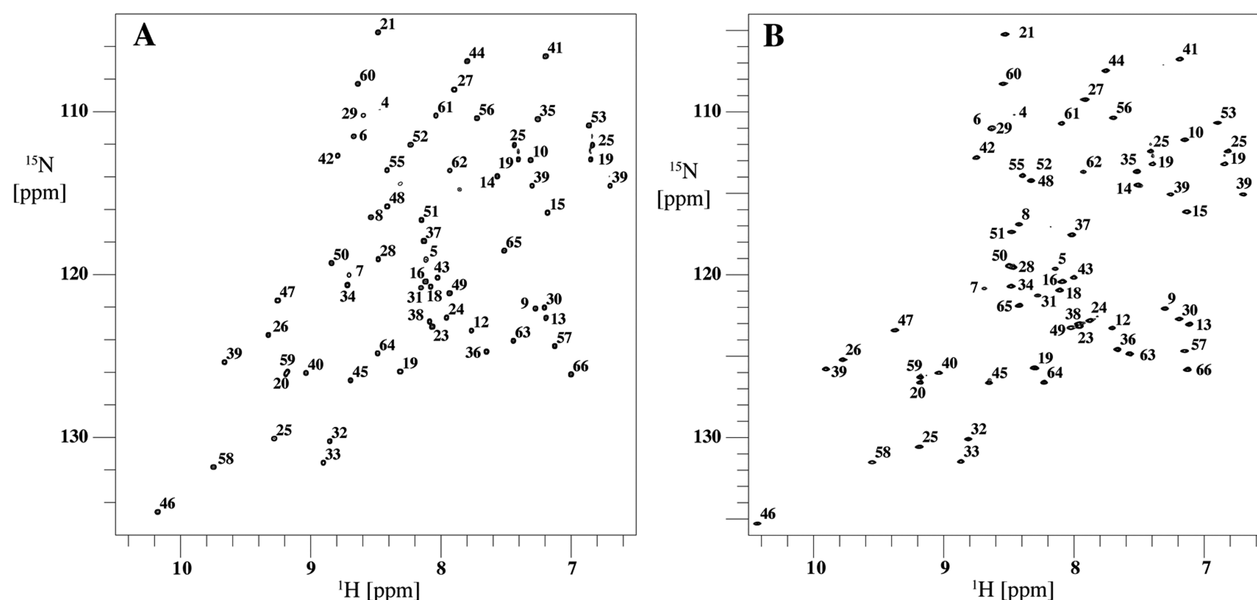

Figure 1. Assignment of Cd_6- and Zn_6-HpCdMT. Assigned $^{15}N-^{1}H$ HSQC spectra of (A) Cd_6-HpCdMT and (B) Zn_6-HpCdMT recorded at 600 MHz, pH 7.0, and 298 K.

the RMSDs were now reasonable, indicating adequate searches of conformational space and removal of any bias in the NOE assignment. To improve the precision further, in the final consensus runs the metal−Cys connectivities determined above were included as explicit restraints.

The topology of cluster formation was investigated by analyzing the Cys-S^{γ}−metal distances in the 20 independent computations as well as in the final structure of the consensus run. For each metal ion, the four shortest distances were selected and used to define the four closest Cys residues as the directly coordinated ones. Statistics of topologies sorted by target function were compiled for the 400 different lowest-energy conformers from 20 runs using different initial starting structures (Tables S1 and S2). One coordination topology was clearly dominant and used for the final consensus calculation by introducing explicit Cys-S^{γ}−metal distance restraints according to that topology while still allowing both chiralities. For the Cd-loaded variant, the precision of the structure was improved by introducing Cys-S^{γ}−metal distance restraints corresponding to observed correlations in the $^{113}Cd-^{1}H$ HSQC-TOCSY spectra already in the 20 independent consensus runs.

Structural refinement of the final consensus bundle in explicit water was performed with Xplor-NIH 2.38[42,43] using its all-hydrogen force field and fixing the positions of all Cd and S^{γ} atoms in the MD run. Structures were analyzed with Procheck[44] and visualized using PYMOL.[45]

Dynamics. Standard ^{15}N relaxation measurements with modified HSQC experiments[46] were performed to describe protein dynamics: ^{15}N longitudinal relaxation times (T_1) using inversion−recovery,[47] ^{15}N spin−lattice relaxation times (T_2) with CPMG,[48] and $^{15}N\{^{1}H\}$ NOE by steady-state NOE.[49] For the determination of T_1 and T_2, a series of spectra were recorded with delays set to 0, 10, 20, 30, 60 (2×), 120, 260, 510, 1210, and 2010 ms for T_1 data and 0, 17 (2×), 34, 51, 68, 102 (2×), 119, 204, and 305 ms for T_2 data. The recycle delay was set to 2 s, and for each t_1 increment, eight scans were recorded. All relaxation data were measured at 600 and 700 MHz on 0.5−1 mM solutions of the corresponding proteins at 298 K. Peaks were integrated, and the resulting peak volumes fitted to monoexponential functions of the type $V = V_0 \exp(-\Delta/T_1)$ using the Levenberg−Marquardt algorithm.[50] The $^{15}N\{^{1}H\}$ NOE values were obtained as peak volume ratios from a pair of spectra with and without proton saturation during the 5 s interscan delay.

Primary and Tertiary Structure Comparisons. Protein sequences of separate N- and C-terminal domains of animal MTs, for which tertiary structures are available, were aligned together with other N- and C-terminal MT sequences of species from the same animal clade for Vertebrata (vertebrates), Echinodermata (sea urchins), Arthropoda (crustaceans), and Mollusca (gastropods) (Table S3). Each alignment contained 10 unique N- or C-terminal sequences, except for Echinodermata (sea urchins), where only five primary sequences are available. N- and C-terminal domain borders were chosen to coincide with the first and last Cys residues of the respective chain. Sequence alignments were obtained with the "muscle" option using the freely accessible program platform SeaView (version 4.7) of PRABI-Doua.[51] For assessment of the normalized global similarity score (S) between clades, the same numbers of aligned sequences (5 or 10) of N- or C-terminal domains were pairwise compared between clades. S values were calculated with the openly accessible program package SIAS (Sequence Identity and Similarity) of the Immunomedicine group of the Universidad Complutense Madrid (http://imed.med.ucm.es/Tools/sias.html) with default settings. Structural alignments were performed using the "align" and "cealign" routines within PYMOL.[45]

■ RESULTS

The Cd- and Zn-containing isotopically labeled variants of HpCdMT were obtained by recombinant protein expression in *E. coli* using minimal media containing $[^{15}N]NH_4Cl$ and, if applicable, $[^{13}C]$glucose as the sole nitrogen and carbon sources, respectively. HpCdMT was expressed as a fusion with glutathione *S*-transferase (GST) and liberated from its fusion partner via thrombin cleavage. The Zn-loaded species was

DOI: 10.1021/acs.biochem.9b00830
Biochemistry 2019, 58, 4570−4581

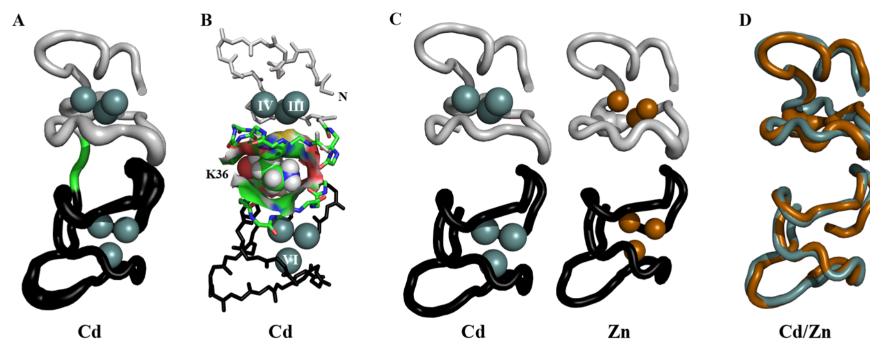

Figure 2. Structures of HpCdMT. (A) Solution structure of Cd_6-HpCdMT. N- and C-terminal domains are colored gray and black, respectively. Cd^{2+} ions are depicted as spheres. The diameter of the tube indicates the structural variability among the 20 lowest-energy conformers after superposition of the Cα atoms of residues 9−65. (B) Single conformer of Cd_6-HpCdMT highlighting the side chain of Lys36, which is located between the two domains. (C) N- and C-terminal domains of Cd_6- and Zn_6-HpCdMT, in which backbone atoms of individual domains from the 20 lowest-energy structures are superimposed. (D) Superposition of the 20 lowest-energy conformers of individual domains of both the Zn- and Cd-loaded forms.

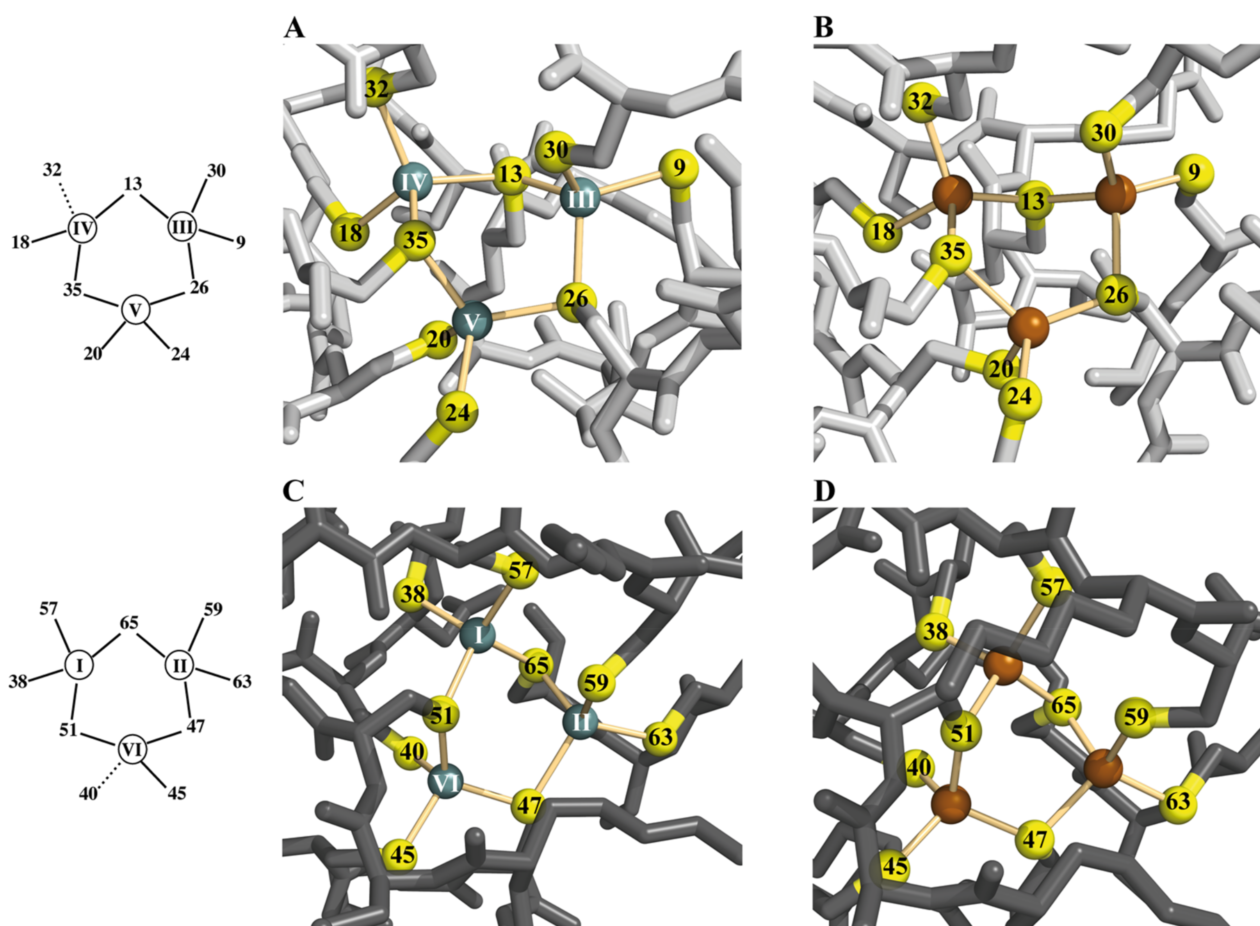

Figure 3. Three-metal cluster topology. Coordination mode of the N-terminal (top) and C-terminal (bottom) domains of (A and C) Cd_6- and (B and D) Zn_6-HpCdMT. Sulfur atoms of coordinating Cys residues are annotated with the corresponding residue numbers. For the sake of clarity, the Cys−Cd connectivities are depicted schematically on the left. Connectivities that cannot be seen in the ^{113}Cd−^{1}H correlation spectra are indicated by dotted lines.

obtained from the corresponding Cd form through metal exchange. Their purity and metal ion content were confirmed by ESI-TOF mass spectrometry.

Resonance Assignments. Chemical shifts were assigned from 3D triple-resonance NMR experiments using standard procedures. Sequential connectivities were established on the basis of HN(CO)CACB/HNCACB[31] spectra. The C^α and C^β chemical shifts together with H^α and H^β shifts from HBHA(CO)NH[30] provided anchoring points for side chain assignment through the use of (H)CCH- and H(C)CH-TOCSY experiments[32,33] supported by ^{13}C- and ^{15}N-resolved NOESY experiments.[34,35] Due to the excellent signal dispersion, almost all nonlabile side chain resonances could be assigned. The C^β and C^γ chemical shifts indicate that the Glu16-Pro17 peptide bond is in the *cis* conformation,[52] as observed by us for the corresponding Pro residues in the two

DOI: 10.1021/acs.biochem.9b00830
Biochemistry 2019, 58, 4570−4581

N-terminal domains of LlMT.[9] Assignment of the Zn-loaded variant (Zn_6-HpCdMT) was largely facilitated by knowledge of assignments from the Cd species but independently verified using data from 3D triple-resonance NMR experiments. For Zn- and Cd-loaded HpCdMT, 97.7% and 95.5% of all observable resonances were assigned, respectively, and representative annotated $^{15}N-^{1}H$ HSQC spectra of both metal forms are depicted in Figure 1.

To establish the metal coordination, distinct correlations between cysteines and Cd^{2+} ions were assigned from $^{113}Cd-^{1}H$ HMQC and ^{1}H-TOCSY-relayed $^{113}Cd-^{1}H$ HMQC spectra (Figure S5).[36,37] The one-dimensional (1D) ^{113}Cd spectrum shows the six expected resonances, of which five are located in the typical chemical shift range for tetrathiolate coordination, while one resonance occurred outside that range at 543 ppm (Figure S6).

Chemical shifts of Cd and Zn species differ slightly with more notable alterations at and in the vicinity of cysteine residues, as observed in other metallothioneins[53] or ^{113}Cd-loaded variants of zinc binding proteins.[54] The carbon shift differences for C^{α} and C^{β} have been added to Figure 5. One significant exception was observed for Glu50, for which carbon differences are remarkably higher than for the other non-cysteine residues. The special behavior of this residue will be further discussed in the context of the relaxation data.

Structure Calculations of Cd- and Zn-Loaded HpCdMT. A central aspect of this work was the question of whether the two variants, despite the different ionic radii of Cd^{2+} and Zn^{2+}, have the same structure and metal coordination mode. While in the case of Cd^{2+} the coordination can be determined experimentally using $^{113}Cd-^{1}H$ correlations, this is not possible for the NMR-silent Zn^{2+}. Therefore, we used the following strategy to determine the structures of the Zn- and Cd-loaded variants of HpCdMT in the absence of an exact knowledge of the coordinating Cys residues. (i) The individual domains are assumed to form three-metal clusters of an architecture that is similar to that of the mammalian β-domains. (ii) Residue library entries for the structure calculation program CYANA were created with dummy atoms at the positions of ligand atoms that place the metal ion in the center of a perfect tetrahedron (see Methods). (iii) Ambiguous distance restraints were applied between these dummy atoms and all Cys-S^{γ} atoms. The metal cluster topology for Cd_6-HpCdMT resulting from this procedure agreed with correlations in the $^{1}H-^{113}Cd$ HMQC-TOCSY spectrum. To refine the structure of Cd_6-HpCdMT, the ambiguous distance restraints were replaced by the specific distance restraints from the Cd correlation spectra. During the first structure calculations, solely NOE-derived upper distance limits were used for the Cd-loaded species. In a second round, ambiguous distance restraints were introduced between ligand dummy atoms and Cys-S^{γ} atoms and explicit metal−metal lower distance bounds were applied. The resulting bundles for both species have low residual restraint violations and low CYANA target function values (Table 1).

Structure of Cd- and Zn-Loaded HpCdMT. The three-dimensional structure of Cd-loaded HpCdMT is characterized by the formation of two distinct nearly spherical domains joined by a short linker comprising residues Lys36 and Thr37 (Figure 2), thereby creating the well-known dumbbell shape. The fold of each domain is determined by a three-metal cluster comprising three Cd^{2+} ions coordinated by nine Cys-S^{γ} atoms (Cd_3Cys_9). The positions of the cysteines define the length of the interconnecting loops. The first nine residues at the N-terminus form a flexible tail that is devoid of Cys residues.

The metal coordination mode and the topology of the N- and C-terminal domains are shown for Cd_6- and Zn_6-HpCdMT in Figure 3. In the N-terminal domain, the protein chain wraps right-handedly around the metal cluster as observed in some other three-metal clusters of MTs.[6−8,37,55−58] In contrast, the handedness changes within the C-terminal domain.

It starts left-handedly for residues 39−58 and becomes right-handed for residues 59−67. This results in a deep cleft containing the cadmium cluster sandwiched between the right- and left-handed loops. The left-handed loop is mainly formed by a series of four consecutive residues, Cys40, -45, -47, and -51, that all coordinate to the same Cd^{2+} ion (Cd-VI), followed by a loop of five non-cysteine amino acids that contains a short helical segment (Pro54-Asp55-Ser56, 3_{10} helix). The protein chain continues right-handed around the two remaining Cd ions of the C-terminal domain. Besides the 3_{10} helix (found in half of the 20 computed models), only bends and turns are present as secondary structure elements throughout the protein. They are common and formally described features of metallothioneins.[59]

The interdomain linker comprising Lys36 and Thr37 is in an extended conformation, and the side chain of Lys36 packs tightly against both domains (Figure 2B), helping to orient them relative to each other. The resulting contacts are supported by a number of interdomain long-range NOEs (Figure S7), which also help to define the conformation in the linker region, resulting in an almost linear arrangement of the two domains and the linker. The two planes spanned by the three Cd ions within each cluster are approximately orthogonal to each other.

The structure of the Zn form of HpCdMT is very similar to that of the Cd-loaded variant. An overlay of the individual domains of both variants shows a backbone RMSD of 0.60 Å for the N-terminal domain (residues 9−35) and 0.34 Å for the C-terminal domain (residues 38−65) (Figure 2D). The Gly27-Glu28-Gly29 and Gly60-Ser61-Ser62 loops are less well-defined in Zn-HpCdMT, and the α-helical stretch in the segment of residues 54−56 is observed in only eight of the 20 models.

Dynamics. To probe internal dynamics, we measured ^{15}N relaxation rates for both metal variants (Figure S8). Due to the fact that peaks in the $^{15}N-^{1}H$ HSQC spectrum are very well separated, spectra could be integrated reliably, and nearly perfect fits with low residual errors were obtained. Moreover, the data were measured on two different samples for both variants, and the values from both measurements are in close agreement.

In general, high values of the $^{15}N\{^{1}H\}$ NOE indicate that the polypeptide chain is fairly rigid in both variants (Figure 4). Lower values (<0.64) are observed for only the N-terminal residues preceding the first Cys9, a longer Pro-containing loop in the N-terminal domain encompassing residues Arg14−Pro17, and the linker region. Similar data for R_1 are observed for the Cd- and Zn-loaded proteins (Figure S8).

While R_1 values are very similar for the Cd- and Zn-containing forms and generally very uniform, increased R_2 values are observed for some residues of the Zn-containing species, implying contributions from conformational exchange (Figure 5). Exceptionally high R_2 values are observed for residues Lys49 and Glu50 next to Cys51.

DOI: 10.1021/acs.biochem.9b00830
Biochemistry 2019, 58, 4570−4581

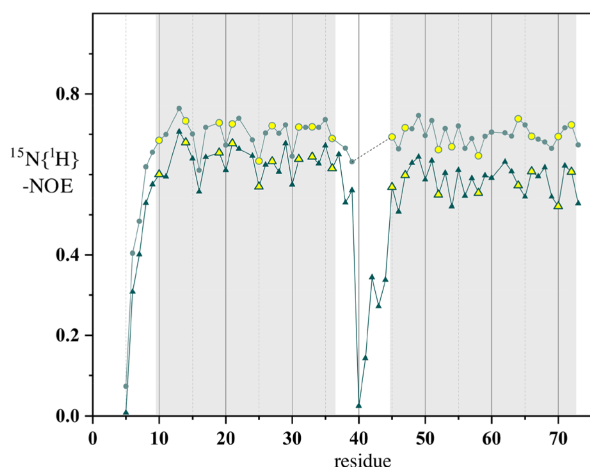

Figure 4. Backbone dynamics of Cd_6-HpCdMT. $^{15}N\{^1H\}$ NOE of HpCdMT with the wild-type linker sequence (KT) (light green lines and spheres) and for HpCdMT with the extended linker from *Megathura crenulata* (*Mc*) (VKTEAKTT) (dark green triangles and lines), HpMcCdMT. Coordinating Cys residues are colored yellow. N- and C-terminal domains are highlighted in gray. Residue numbering refers to the *Mc* variant.

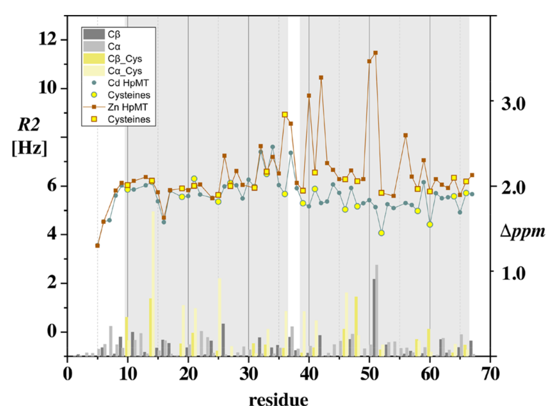

Figure 5. Comparison of transverse relaxation rates. Transverse relaxation rates (left *y*-axis) are depicted for Cd-loaded (green circles and lines) and Zn-loaded (orange squares and lines) forms of HpCdMT. ^{13}C chemical shift differences [$\Delta\delta = |\delta(Cd) - \delta(Zn)|$] are shown as bars (right *y*-axis). The positions of cysteines are colored yellow. N- and C-terminal domains are highlighted in gray.

Interestingly, this was also seen for Asn39−Thr41 enclosing Cys40, which in some of the computed structures served as an alternative for Cys51 as a bridging residue. Moreover, Cys35, the last Cys residue of the N-terminal domain, and the linker residue Lys36 display higher R_2 values, suggesting participation of the linker region in conformational exchange. As expected, R_2 rates are larger at 16.4 T than at 14.1 T, supporting the presence of exchange (Figure S8).

To determine the influence of the linker length for protein stability, a modified Cd variant, HpMcCdMT, was created containing the eight-residue linker of the snail *Megathura crenulata* (VKTEAKTT) as compared to the two-residue *H. pomatia* KT sequence. The comparison of $^{15}N\{^1H\}$ NOE values reveals generally lower values in the extended linker mutant (Figure 4). Within the two individual domains, the data are again fairly uniform. As in the *L. littorea* metallothionein,[9] we interpret this observation as a motional decoupling of the two domains, which now tumble independently and therefore faster, resulting in lower $^{15}N\{^1H\}$ NOE values. The fact that heteronuclear NOEs are uniform in both domains indicates that the backbone of the individual domains is not destabilized compared to the wild-type protein. We therefore conclude that interdomain contacts are not required for the high conformational stability of this protein.

A comparison of the structures and dynamics of the Cd and Zn forms of HpCdMT reveals recurring extraordinary features for residues 36−51 that include linker residues Lys36 and Thr37 and all four Cys residues that coordinate to Cd-IV. The latter is characterized by an unusual ^{113}Cd upfield shift of 513 ppm. Moreover, residues in this region display strongly increased R_2 rates indicating the presence of exchange in the Zn form. The C^α and C^β chemical shift differences between the Cd and Zn forms of Glu50 are 5 times the average of all non-Cys and 2 times the average of Cys residues.

■ DISCUSSION

The highly unusual amino acid composition and the unclear role of metallothioneins in biological systems attracted much interest in the structures of these small proteins.[60] MTs are known to bind a variety of different, mostly divalent metal ions such as Zn^{2+}, Cd^{2+}, and Hg^{2+} but also monovalent Cu^{+}.[1,4,5,61,62] While the exact role of MTs is still under discussion and likely dependent on organism and possibly also dependent on tissue and isoform, one frequently claimed function of MTs is the involvement in heavy metal detoxification.[63] As Blindauer and Leszczyszyn describe in their review, metallothioneins are much more than "metal sponges" in that they "play an integral role in the trafficking and homeostasis of essential metal ions" by taking them up or leasing them in a controlled fashion.[5]

Often MTs bind different metals with similar affinities. Usually, MTs of mixed metal compositions are isolated *in vivo*, where they are exposed to a cocktail of different metal ions.[64,65] Similar observations are made when expressing metallothioneins recombinantly, using media containing both Zn^{2+} or Cd^{2+} and Cu^{2+} ions.[66] Interestingly, some species have developed MTs with high metal specificity, e.g., the snail *H. pomatia*.[16] Three different MT isoforms were discovered in pulmonate and snails of the helicid family, namely, in *H. pomatia* and *Cornu aspersum*: one being selective for Cd^{2+} (HpCdMT and CaCdMT, respectively), with a high affinity also for Zn^{2+}, especially after recombinant expression *in vitro*, one being specific for Cu^{+} (HpCuMT and CaCuMT, respectively), and one without metal specificity (HpCd/CuMT and CaCd/CuMT, respectively).[14,20,67,68] We suspect that these metal-specific MT isoforms developed during evolution to help adapting to environments with elevated levels of these metals. Interestingly, these selectivities seem to partially contradict the chemical rules of the Irving−Williams series with an established affinity hierarchy of Cu > Cd > Zn.[69] Apparently, the metal binding preferences of snail MTs are determined by not only their metal ion affinities for the sulfur atoms of the Cys residues but also the chemical nature of the nearby non-Cys residues, which are able to overcompensate for these rules by modifying the accessibility of different metal ions to the sulfur binding sites.[20] The positions of the metal-coordinating Cys residues are fully conserved between these isoforms, suggesting that they are derived from a common ancestral protein. In this work, we set out to determine the structures of HpCdMT loaded with Cd^{2+} and with Zn^{2+} to

DOI: 10.1021/acs.biochem.9b00830
Biochemistry 2019, 58, 4570−4581

Table 2. Structural Comparison of MTs[a]

	cluster topology[b]	N/C[c]	PDB	N[c] RMSD (Å)		C[c] RMSD (Å)	
				Cys-S^{γ}	C^{α}	Cys-S^{γ}	C^{α}
gastropod	[1 2 6 7] [2 3 8 9] [4 5 6 9]	N	5ml1_N1	0.56	1.62	3.78	6.00
			5ml1_N2	0.28	0.97	4.02	6.56
crustacea	[1 2 6 7] [2 3 8 9] [4 5 6 9]	C	1dmc	0.34	5.25	3.24	5.92
			1j5l	0.39	5.40	3.24	6.57
	[1 2 5 6] [2 3 7 8] [3 5 8 9]	N	1dme	3.10	4.77	2.96	5.51
			1j5m	2.97	4.55	3.15	5.47
sea urchin	[1 2 5 6] [2 7 8 9] [3 4 5 9]	C	1qjl	3.56	4.05	3.19	6.70
vertebrate	[1 2 6 7] [2 3 4 8] [4 5 7 9]	N	1m0j	1.46	3.97	3.64	3.67
			2mhu	1.76	2.34	3.10	5.42

[a]RMSDs are calculated by superimposing C^{α} or S^{γ} atoms of N-terminal (columns 5 and 6) or C-terminal (columns 7 and 8) domains of the lowest-energy conformer of HpCdMT with corresponding MTs specified in column 1. Only residues between the first and last Cys from a domain are included to exclude flexible parts. [b]Numbers refer to the order of Cys residues: 1 means "first Cys in sequence". Underlined residues coordinate to two different metals (bridging). [c]"N"- or "C"-terminal domain.

Table 3. Comparison of the Gastropod Topology to Four-Metal Clusters

	cluster topology[a]	N/C[b]	PDB	N[b] RMSD (Å)		C[b] RMSD (Å)	
				Cys-S^{γ}	C^{α}	Cys-S^{γ}	C^{α}
gastropod	[1 5 6 9] [**2 3** 4 5] [4 7 8 9]	C	5ml1_C	3.91	4.91	1.15	1.13
sea urchin	[1 3 4 7] [**5 6** 7 8] [1 8 9 10] [2 4 10 11]	N	1qjk	4.31	7.37	3.13	4.94
vertebrate	[1 2 6 7] [2 3 4 8] [4 5 6 11] [8 **9 10** 11]	C	1m0g	3.26	7.85	3.46	4.86

[a]Numbers refer to the order of Cys residues: 1 means "first Cys in sequence". Underlined residues are coordinating to two different metals (bridging). Clusters, in which connected Cys are consecutive, are shown in bold. [b]"N"- or "C"-terminal domain.

advance our understanding of how metal specificity is obtained in these proteins.

The solution structure of the cadmium-specific metallothionein of the gastropod *H. pomatia*, HpCdMT, binding either Cd^{2+} or Zn^{2+}, shows two three-metal clusters with a topology similar to that originally observed in three-metal domains of vertebrate MTs (Table 2).[37,55−58] For comparison, see the topologies of four-metal clusters of MTs in Table 3.

The N-terminal domain reveals essentially the same fold as the α1 and α2 domains of the formerly reported Cd_9-LlMT[9] (with C^{α} RMSDs of 0.97 and 1.62 Å, respectively) and also the C-terminal domains of Cd_6-HpCdMT and Cd_9-LlMT superimpose well [with a C^{α} RMSD of 1.13 Å (Figure S9)]. A comparison of the amino acid sequences of the C-terminal domains of HpCdMT and LlMT reveals that in addition to the coordinating Cys several segments of the C-terminal domain are identical. However, the Cys-spacing residues following the linker differ, and in this region, the backbone is slightly more flexible in LlMT as reflected in a small but significant decrease in the $^{15}N\{^{1}H\}$-NOE values by 0.1−0.2 for residues 74−76. This part also shows the greatest structural difference (RMSD of 1.7 Å for residues 76−87 vs RMSD of 0.6 Å for residues 88−101). In the C-terminal domain of HpCdMT, four consecutive cysteine residues (Cys40, -45, -47, and -51) coordinate the same metal, which to the best of our knowledge is unique in three-metal clusters but common in four-metal cluster domains, e.g., in sea urchin[6] and vertebrate MTs.[37,55−58] HpCdMT also features two consecutive bridging cysteines (47 and 51), which disagrees with rules derived from formerly known three-metal clusters, where two bridging cysteine residues are always separated by at least one nonbridging residue.[6] Interestingly, this uncommon topology involves Cd-VI that is characterized by an unusually upfield-shifted resonance at 543 ppm (in LlMT, the analogue Cd is even shifted to 516 ppm). We suspect that at least one of the Cys residues is only transiently coordinated to the corresponding Cd^{2+} ion, and therefore, the coordination mode may not be uniquely defined. When the linker KT is replaced by the extended VKTEAKTT sequence of *M. crenulata*, the $^{15}N\{^{1}H\}$ NOE drops, likely because the domains lose their mutual contacts and become motionally decoupled. As in LlMT, individual domains are still well folded even when contacts between the domains are no longer formed.

No significant structural differences were observed between the Zn- and Cd-loaded forms of HpCdMT with the exception that the two domains seem to be slightly differently oriented relative to each other. However, ^{15}N relaxation data reveal the presence of conformational exchange contributions to transverse relaxation in the Zn species, indicating that the protein might have been optimized for binding Cd^{2+} and not Zn^{2+} during evolution (R. Dallinger et al., manuscript submitted for publication). We have made similar observations for LlMT, in which exchange contributions to R_2 were again detected only in the Zn form.[9] The fact that the Cd cluster is 20% larger in volume increases the size of the individual domains slightly,[70] and we suspect that the differences in relative domain orientations are due to this fact, in particular considering that interdomain contacts are formed in HpCdMT. It is further remarkable that Glu50 is the residue that shows the largest ^{13}C chemical shift difference between the Cd and Zn forms of HpCdMT. Upon comparison of the C-terminal domains of LlMT and HpCdMT, this position is one of the few substituted ones compared to HpCdMT, being replaced by a Gly residue with quite different side chain requirements.

A summary of the structural similarities in terms of RMSDs for superposition of C^{α} atoms of known MT structures is presented in Figure 6A.

Cadmium binding metallothioneins of closely related organisms with identical locations of coordinating Cys residues tend to create clusters with the same topology. The topologies

DOI: 10.1021/acs.biochem.9b00830
Biochemistry 2019, 58, 4570−4581

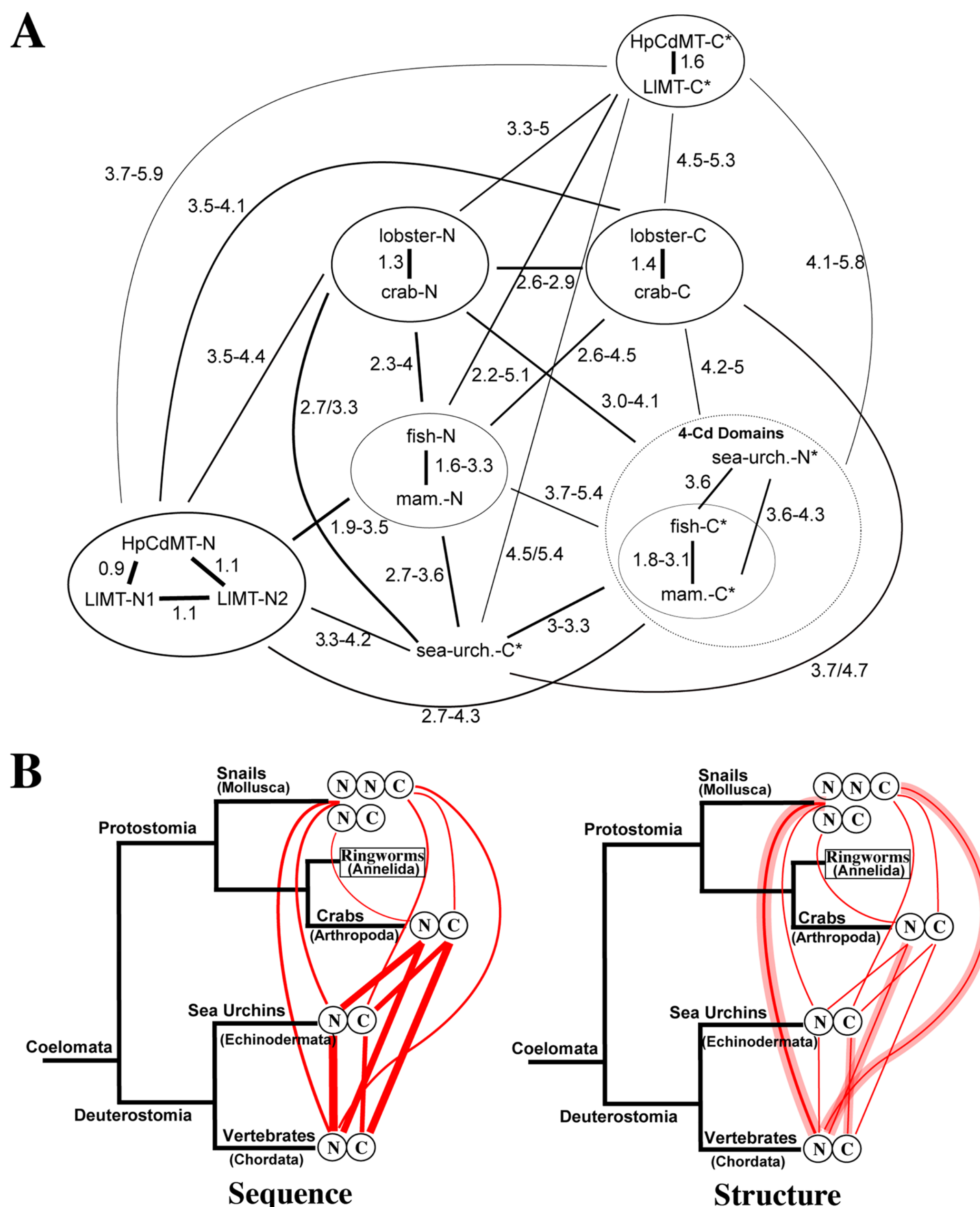

Figure 6. Relationships of known MT structures. (A) Structural comparison of known MT domains. Values present RMSDs when superimposing Cα atoms. Upon comparison with more than one MT structure, ranges instead of single values are presented. The asterisk indicates that the sign of *z*-coordinates was inverted to create the mirror image. Thicker lines indicate more similarity (lower RMSDs). (B) Comparison of sequence (left) and structure (right) similarities of MT N- and C-terminal domains for animal clades within the informal group of coelomata (bilaterian animals with a main body cavity), which comprises all species for which MT 3D structures have published so far. The thickness of the lines is proportional to the "global similarity index" (*S*) (left) or inversely proportional to the RMSD. When ranges of RMSD exist, transparent and solid lines present higher and lower values, respectively.

of the two Crustacea species, blue crab (*C. sapidus*)[7] and lobster (*H. americanus*),[8] are identical (1.4 Å RMSD when superimposing either the N- or C-terminal domains) as well as the two cadmium binding metallothioneins from the vertebrate species black rockcod (*Notothenia coriiceps*), a fish, and human MT2 (Table 2) (RMSDs of 2.0 and 2.4 Å for N- and C-terminal domains, respectively). Surprisingly, the N-terminal domain of Cd_6-HpCdMT has the same cluster topology as the C-terminal domain from the two Crustacea species, blue crab[7] and lobster,[8] although Cys residues are observed at different positions. Upon superimposition of the coordinating S^{γ}-Cys atoms, they agree well with RMSDs of 0.34 Å for blue crab and 0.39 Å RMSD for lobster MT, indicating that the ring pucker is similar while the fold of the protein backbone is quite different (C^{α} RMSDs of 5.25 Å for blue crab and 5.40 Å for lobster MT). For representative superpositions, see also Figure S10.

Interestingly, the backbone fold of the N-terminal domain of HpCdMT is more similar to the β domain of vertebrates, in particular to human MT2 (2.2 Å) than to the corresponding three-metal domains of crustacean (4.4 or 5.3 Å) or sea urchin (6.2 Å) MTs. This is in contrast to the otherwise low degree of similarity of primary MT sequences (for both N- and C-terminal domains) between the clades of Gastropoda (representing the Mollusca) and Vertebrata, indicating that

DOI: 10.1021/acs.biochem.9b00830
Biochemistry 2019, 58, 4570−4581

structural requirements for coordinating the metal ions in a cluster of given topology result in convergent 3D architectures, even among phylogenetically highly divergent clades (Figure 6B). Another interesting observation is that sometimes much better superpositions are obtained when one domain is superimposed with the mirror image of another domain, indicating that the overall fold is similar but the polypeptide chain wraps around the metal cluster in an opposite sense.[6]

We also briefly comment on an important technical aspect of this study. Most of the presently available structural knowledge is derived from solution NMR studies because crystallization of MTs proved to be difficult.[5,58] However, MTs have a peculiarity in that they usually have neither regular secondary structure nor direct contacts between distant parts of the polypeptide chain. As a consequence, few of the structurally important long-range NOEs due to such contacts can be observed. To obtain sufficient restraints for structure calculations, direct Cys-H^{β}—metal scalar couplings are measured to establish the metal coordination sphere.[36,71,72] While this worked well in many cases, internal cluster dynamics may broaden metal resonances beyond detection. In addition, such H^{β} (Cys)—metal scalar couplings can be measured for only NMR-active $S = {}^{1}/_{2}$ metal nuclei such as ^{113}Cd, ^{111}Cd, and ^{199}Hg but not for the biologically relevant Zn. Therefore, Zn^{2+} has mostly been replaced by Cd^{2+} in these studies assuming that the cluster topology is identical.[53] However, the ionic radii of Zn^{2+} (0.74 Å) and Cd^{2+} (0.92 Å) differ, accounting for a 20% difference in the volumes of the clusters.[70] Moreover, the more polarizable (softer) Cd^{2+} forms stronger bonds to sulfur than Zn^{2+}, resulting in lower dissociation constants. For these reasons, a method that does not rely on a quasi-isomorphous replacement of Zn by Cd is preferable.

Herein, we demonstrate that the structure of Cd_6-HpCdMT can be determined without the inclusion of specific metal—cysteine NMR restraints by enforcing tetrahedral coordination geometry and using ambiguous metal—Cys restraints in the structure calculations. This approach assumes knowledge of the geometry of the Cys—metal complexes but is independent of any experimental proton—metal correlations. It combines the efforts to achieve high-resolution metallothionein structures without metal restraints for complexes with NMR-inactive nuclei, e.g., for Cu or Zn,[73,74] and the traditional way of metallothionein distance geometry calculations to fix tetrahedral symmetry by measured Cd—Cys connectivities.[36,75] Key to success was a nearly complete assignment of backbone and side chain resonances and high-quality NOESY spectra that contained a large fraction of the scarce long-range NOEs characteristic for this family of proteins.

■ CONCLUSIONS

Herein, we have demonstrated that structures of metallothions can be determined without using explicit metal—thiolate restraints derived from measurements of scalar proton—cadmium couplings in Cd-loaded species. This indicates an avenue for determining structures of other MTs where isostructural replacements of the metal by the NMR-active cadmium are not possible, e.g., for Cu-loaded forms. Our studies have also indicated that the CdMT species of *H. pomatia* has been optimized for Cd versus Zn binding. Apparently, evolution has come up with similar coordination geometries from relatively different amino acid sequences, and sometimes, the degree of similarity of folds is higher for evolutionarily more remotely than for the more closely related species.

■ ASSOCIATED CONTENT

Supporting Information

The Supporting Information is available free of charge on the ACS Publications website at DOI: 10.1021/acs.biochem.9b00830.

> Annotated ^{15}N—^{1}H HSQC spectra of Cd-HpCdMT and Zn-HpCdMT, 1D ^{113}Cd and 2D ^{113}Cd—^{1}H correlation spectra, plots of long-range distance restraints, further details about the structure calculations, complete set of (R_1, R_2, and ^{15}N{^{1}H} NOE) relaxation rates, superpositions of domains from different organisms, and sequence alignments (PDF)

Accession Codes

The coordinates and chemical shifts of Cd_6- and Zn_6-HpMT have been deposited in the Protein Data Bank as entries 6QK6 and 6QK5, respectively, and in the BMRB database as accession codes 34356 and 34355, respectively.

■ AUTHOR INFORMATION

Corresponding Authors

*E-mail: oliver.zerbe@chem.uzh.ch.
*E-mail: reinhard.dallinger@uibk.ac.at.

ORCID

Òscar Palacios: 0000-0002-2987-7303
Oliver Zerbe: 0000-0003-0475-438X

Present Address

[@]R.W.: Astex Pharmaceuticals, 436 Cambridge Science Park, Milton Road, Cambridge CB4 0QA, U.K.

Funding

This work was generously supported by a cooperation DACH grant to R.D. and O.Z. from the Austrian Science Fund and the Swiss National Science Foundation (Dach Project Grant I 1482-N28). Ò.P. and M.C. also acknowledge the financial support of the Spanish Ministerio de Ciencia e Innovación and FEDER through Project BIO2015-67358-C2-2-P.

Notes

The authors declare no competing financial interest.
[∇]Deceased December 5, 2016.

■ ACKNOWLEDGMENTS

The authors especially thank Christian Baumann for helpful discussion and critical reading.

■ REFERENCES

(1) Kägi, J. H. R., and Schäffer, A. (1988) Biochemistry of metallothionein. *Biochemistry 27*, 8509—8515.
(2) Blindauer, C. A. (2008) Metallothioneins with unusual residues: histidines as modulators of zinc affinity and reactivity. *J. Inorg. Biochem. 102*, 507—521.
(3) Kägi, J. H. R. (1993) Evolution, structure and chemical activity of class I metallothioneins: an overview. In *Metallothionein III* (Suzuki, K. T., Imura, N., and Kimura, M., Eds.) pp 29—55, Birkhäuser Verlag, Basel, Switzerland.
(4) Romero-Isart, N., and Vašák, M. (2002) Advances in the structure and chemistry of metallothioneins. *J. Inorg. Biochem. 88*, 388—396.
(5) Blindauer, C. A., and Leszczyszyn, O. I. (2010) Metallothioneins: unparalleled diversity in structures and functions for metal ion homeostasis and more. *Nat. Prod. Rep. 27*, 720—741.

DOI: 10.1021/acs.biochem.9b00830
Biochemistry 2019, 58, 4570—4581

(6) Riek, R., Prêcheur, B., Wang, Y., Mackay, E. A., Wider, G., Güntert, P., Liu, A., Kägi, J. H. R., and Wüthrich, K. (1999) NMR structure of the sea urchin (Strongylocentrotus purpuratus) metallothionein MTA. *J. Mol. Biol. 291*, 417−428.
(7) Narula, S. S., Brouwer, M., Hua, Y., and Armitage, I. M. (1995) Three-dimensional solution structure of Callinectes sapidus metallothionein-1 determined by homonuclear and heteronuclear magnetic resonance spectroscopy. *Biochemistry 34*, 620−631.
(8) Muñoz, A., Forsterling, F. H., Shaw, C. F., and Petering, D. H. (2002) Structure of the $^{113}Cd_3$ beta domains from Homarus americanus metallothionein-1: hydrogen bonding and solvent accessibility of sulfur atoms. *J. Biol. Inorg. Chem. 7*, 713−724.
(9) Baumann, C., Beil, A., Jurt, S., Niederwanger, M., Palacios, O., Capdevila, M., Atrian, S., Dallinger, R., and Zerbe, O. (2017) Structural Adaptation of a Protein to Increased Metal Stress: NMR Structure of a Marine Snail Metallothionein with an Additional Domain. *Angew. Chem., Int. Ed. 56*, 4617−4622.
(10) Dallinger, R., Berger, B., Gruber, C., Hunziker, P., and Sturzenbaum, S. (2000) Metallothioneins in terrestrial invertebrates: structural aspects, biological significance and implications for their use as biomarkers. *Cell. Mol. Biol. 46*, 331−346.
(11) Janssens, T. K., Roelofs, D., and Van Straalen, N. M. (2009) Molecular mechanisms of heavy metal tolerance and evolution in invertebrates. *Insect Sci. 16*, 3−18.
(12) Brouwer, M., Winge, D. R., and Gray, W. R. (1989) Structural and functional diversity of copper-metallothioneins from the American lobster Homarus americanus. *J. Inorg. Biochem. 35*, 289−303.
(13) Jenny, M. J., Ringwood, A. H., Schey, K., Warr, G. W., and Chapman, R. W. (2004) Diversity of metallothioneins in the American oyster, Crassostrea virginica, revealed by transcriptomic and proteomic approaches. *Eur. J. Biochem. 271*, 1702−1712.
(14) Dallinger, R., Berger, B., Hunziger, P., and Kägi, J. H. R. (1997) Metallothionein in snail Cd and Cu metabolism. *Nature 388*, 237−238.
(15) Berger, B., Dallinger, R., Gehrig, P., and Hunziker, P. E. (1997) Primary structure of a copper-binding metallothionein isoform from mantle tissue of the terrestrial gastropod Helix pomatia. *Biochem. J. 328*, 219−224.
(16) Chabicovsky, M., Niederstätter, H., Thaler, R., Hödl, E., Parson, W., Rossmanith, W., and Dallinger, R. (2003) Localisation and quantification of Cd- and Cu-specific metallothionein isoform mRNA in cells and organs of the terrestrial gastropod Helix pomatia. *Toxicol. Appl. Pharmacol. 190*, 25−36.
(17) Dallinger, R., Chabicovsky, M., Hödl, E., Prem, C., Hunziker, P., and Manzl, C. (2005) Copper in Helix pomatia (Gastropoda) is regulated by one single cell type: differently responsive metal pools in rhogocytes. *Am. J. Physiol. Regul. Integr. Comp.Physiol. 289*, R1185−1195.
(18) Dallinger, R., Berger, B., Hunziker, P. E., Birchler, N., Hauer, C. R., and Kägi, J. H. R. (1993) Purification and primary structure of snail metallothionein. Similarity of the N-terminal sequence with histones H4 and H2A. *Eur. J. Biochem. 216*, 739−746.
(19) Egg, M., Höckner, M., Brandstätter, A., Schuler, D., and Dallinger, R. (2009) Structural and bioinformatic analysis of the Roman snail Cd-Metallothionein gene uncovers molecular adaptation towards plasticity in coping with multifarious environmental stress. *Mol. Ecol. 18*, 2426−2443.
(20) Palacios, Ò., Pagani, A., Pérez-Rafael, S., Egg, M., Höckner, M., Brandstätter, A., Capdevila, M., Atrian, S., and Dallinger, R. (2011) Shaping mechanisms of metal specificity in a family of metazoan metallothioneins: evolutionary differentiation of mollusc metallothioneins. *BMC Biol. 9*, 4.
(21) Wang, H., Zhang, Q., Cai, B., Li, H., Sze, K. H., Huang, Z. X., Wu, H. M., and Sun, H. (2006) Solution structure and dynamics of human metallothionein-3 (MT-3). *FEBS Lett. 580*, 795−800.
(22) Zheng, Q., Yang, W. M., Yu, W. H., Cai, B., Teng, X. C., Xie, Y., Sun, H. Z., Zhang, M. J., and Huang, Z. X. (2003) The effect of the EAAEAE insert on the property of human metallothionein-3. *Protein Eng. Des. Sel. 16*, 865−870.
(23) Pagani, A., Villarreal, L., Capdevila, M., and Atrian, S. (2007) The Saccharomyces cerevisiae Crs5 Metallothionein metal-binding abilities and its role in the response to zinc overload. *Mol. Microbiol. 63*, 256−269.
(24) Live, D. H., Davis, D. G., Agosta, W. C., and Cowburn, D. (1984) Observation of 1000-fold Enhancement of ^{15}N NMR via Proton-Detected Multiple-Quantum Coherences: Studies of Large Peptides. *J. Am. Chem. Soc. 106*, 6104−6105.
(25) Keller, R. (2004) *The Computer Aided Resonance Assignment*, Cantina Verlag, Goldau, Switzerland.
(26) States, D. J., Haberkorn, R. A., and Ruben, D. J. (1982) A Two-Dimensional Nuclear Overhauser Experiment with Pure Absorption Phase in Four Quadrants. *J. Magn. Reson. 48*, 286−292.
(27) Marion, D., and Wüthrich, K. (1983) Application of phase sensitive two-dimensional correlated spectroscopy (COSY) for measurements of ^1H-^1H spin-spin coupling constants in proteins. *Biochem. Biophys. Res. Commun. 113*, 967−974.
(28) Kay, L. E., Keifer, P., and Saarinen, T. (1992) Pure absorption gradient enhanced heteronuclear single quantum correlation spectroscopy with improved sensitivity. *J. Am. Chem. Soc. 114*, 10663−10665.
(29) Palmer, A. G. I. I. I., Cavanagh, J., Wright, P. E., and Rance, M. (1991) Sensitivity improvement in proton-detected two-dimensional heteronuclear correlation NMR spectroscopy. *J. Magn. Reson. 93*, 151−170.
(30) Grzesiek, S., and Bax, A. (1993) Amino acid type determination in the sequential assignment procedure of uniformly ^{13}C/^{15}N-enriched proteins. *J. Biomol. NMR 3*, 185−204.
(31) Shan, X., Gardner, K. H., Muhandiram, D. R., Rao, N. S., Arrowsmith, C. H., and Kay, L. E. (1996) Assignment of N-15, C-13(alpha), C-13(beta), and HN resonances in an N-15, C-13, H-2 labeled 64 kDa trp repressor-operator complex using triple-resonance NMR spectroscopy and H-2-decoupling. *J. Am. Chem. Soc. 118*, 6570−6579.
(32) Bax, A., Clore, G. M., Driscoll, P. C., Gronenborn, A. M., Ikura, M., and Kay, L. E. (1990) Practical aspects of proton-carbon-carbon-proton three-dimensional correlation spectroscopy of ^{13}C labelled proteins. *J. Magn. Reson. 87*, 620−627.
(33) Olejniczak, E. T., Xu, R. X., and Fesik, S. W. (1992) A 4D HCCH-TOCSY experiment for assigning the side chain ^1H and ^{13}C resonances of proteins. *J. Biomol. NMR 2*, 655−659.
(34) Muhandiram, D. R., Farrow, N. A., Xu, G. Y., Smallcombe, S. H., and Kay, L. E. (1993) A gradient C-13 NOESY-HSQC experiment for recording NOESY spectra of C-13 labeled proteins dissolved in H_2O. *J. Magn. Reson., Ser. B 102*, 317−321.
(35) Marion, D., Driscoll, P. C., Kay, L. E., Wingfield, P. T., Bax, A., Gronenborn, A. M., and Clore, G. M. (1989) Overcoming the Overlap Problem in the Assignment of ^1H NMR Spectra of Larger Proteins by Use of Three-Dimensional Heteronuclear ^1H-^{15}N Hartmann-Hahn Multiple-Quantum Coherence and Nuclear Overhauser-Multiple Quantum Coherence Spectroscopy: Application to Interleukin 1b. *Biochemistry 28*, 6150−6156.
(36) Frey, M. H., Wagner, G., Vašák, M., Soerensen, O. W., Neuhaus, D., Wörgötter, E., Kägi, J. H. R., Ernst, R. R., and Wüthrich, K. (1985) Polypeptide metal cluster connectivities in metallothionein-2 by novel H-1-Cd-113 heteronuclear two-dimensional NMR experiments. *J. Am. Chem. Soc. 107*, 6847−6851.
(37) Vašák, M., Wörgötter, E., Wagner, G., Kägi, J. H. R., and Wüthrich, K. (1987) Metal co-ordination in rat liver metallothionein-2 prepared with or without reconstitution of the metal clusters, and comparison with rabbit liver metallothionein-2. *J. Mol. Biol. 196*, 711−719.
(38) Güntert, P., Mumenthaler, C., and Wüthrich, K. (1997) Torsion angle dynamics for NMR structure calculation with the new program DYANA. *J. Mol. Biol. 273*, 283−298.

DOI: 10.1021/acs.biochem.9b00830
Biochemistry 2019, 58, 4570−4581

(39) Güntert, P., and Buchner, L. (2015) Combined automated NOE assignment and structure calculation with CYANA. *J. Biomol. NMR 62*, 453−471.
(40) Vranken, W. F., Boucher, W., Stevens, T. J., Fogh, R. H., Pajon, A., Llinas, M., Ulrich, E. L., Markley, J. L., Ionides, J., and Laue, E. D. (2005) The CCPN data model for NMR spectroscopy: development of a software pipeline. *Proteins: Struct., Funct., Genet. 59*, 687−696.
(41) Buchner, L., and Güntert, P. (2015) Increased reliability of nuclear magnetic resonance protein structures by consensus structure bundles. *Structure 23*, 425−434.
(42) Schwieters, C. D, Kuszewski, J. J, Tjandra, N., and Marius Clore, G (2003) The Xplor-NIH NMR molecular structure determination package. *J. Magn. Reson. 160*, 65−73.
(43) Nederveen, A. J., Doreleijers, J. F., Vranken, W., Miller, Z., Spronk, C. A., Nabuurs, S. B., Güntert, P., Livny, M., Markley, J. L., Nilges, M., Ulrich, E. L., Kaptein, R., and Bonvin, A. M. (2005) RECOORD: a recalculated coordinate database of 500+ proteins from the PDB using restraints from the BioMagResBank. *Proteins: Struct., Funct., Genet. 59*, 662−672.
(44) Laskowski, R. A., MacArthur, M. W., Moss, D. S., and Thornton, J. M. (1993) PROCHECK: a program to check the stereochemical quality of protein structures. *J. Appl. Crystallogr. 26*, 283−291.
(45) DeLano, W. L. (2002) *PyMOL Molecular Graphics System*, DeLano Scientific, San Carlos, CA.
(46) Jurt, S., and Zerbe, O. (2012) A study on the influence of fast amide exchange on the accuracy of ^{15}N relaxation rate constants. *J. Biomol. NMR 54*, 389−400.
(47) Vold, R. L., Waugh, J. S., Klein, M. P., and Phelps, D. E. (1968) Measurement of spin relaxation in complex systems. *J. Chem. Phys. 48*, 3831−3832.
(48) Meiboom, S., and Gill, D. (1958) Modified spin-echo method for measuring spin-relaxation rates. *Rev. Sci. Instrum. 29*, 688−691.
(49) Noggle, J. H., and Schirmer, R. E. (1971) *Nuclear Overhauser Effect - Chemical Applications*.
(50) Press, W. H., Teukolsky, S. A., Vetterling, W. T., and Flannery, B. P. (1992) *Numerical Recipes. The Art of Scientific Computing*.
(51) Gouy, M., Guindon, S., and Gascuel, O. (2010) SeaView version 4: A multiplatform graphical user interface for sequence alignment and phylogenetic tree building. *Mol. Biol. Evol. 27*, 221−224.
(52) Schubert, M., Labudde, D., Oschkinat, H., and Schmieder, P. (2002) A software tool for the prediction of Xaa-Pro peptide bond conformations in proteins based on ^{13}C chemical shift statistics. *J. Biomol. NMR 24*, 149−154.
(53) Messerle, B. A., Schäffer, A., Vašák, M., Kägi, J. H. R., and Wüthrich, K. (1992) Comparison of the solution conformations of human [Zn_7]-metallothionein-2 and [Cd_7]-metallothionein-2 using nuclear magnetic resonance spectroscopy. *J. Mol. Biol. 225*, 433−443.
(54) van Roon, A. M., Yang, J. C., Mathieu, D., Bermel, W., Nagai, K., and Neuhaus, D. (2015) ^{113}Cd NMR experiments reveal an unusual metal cluster in the solution structure of the yeast splicing protein Bud31p. *Angew. Chem., Int. Ed. 54*, 4861−4864.
(55) Arseniev, A., Schultze, P., Wörgötter, E., Braun, W., Wagner, G., Vašák, M., Kägi, J. H. R., and Wüthrich, K. (1988) Three-dimensional structure of rabbit liver [Cd_7]metallothionein-2a in aqueous solution determined by nuclear magnetic resonance. *J. Mol. Biol. 201*, 637−657.
(56) Braun, W., Wagner, G., Wörgötter, E., Vašák, M., Kägi, J. H. R., and Wüthrich, K. (1986) Polypeptide fold in the two metal clusters of metallothionein-2 by nuclear magnetic resonance in solution. *J. Mol. Biol. 187*, 125−129.
(57) Messerle, B. A., Schäffer, A., Vašák, M., Kägi, J. H. R., and Wüthrich, K. (1990) Three-dimensional structure of human [$^{113}Cd_7$]-metallothionein-2 in solution determined by nuclear magnetic resonance spectroscopy. *J. Mol. Biol. 214*, 765−779.
(58) Wüthrich, K. (1991) Determination of the three-dimensional structure of metallothioneins by nuclear magnetic resonance spectroscopy in solution. *Methods Enzymol. 205*, 502−520.
(59) Wagner, G., Neuhaus, D., Wörgötter, E., Vašák, M., Kägi, J. H. R., and Wüthrich, K. (1986) Nuclear magnetic resonance identification of half-turn and 3(10)-helix secondary structure in rabbit liver metallothionein-2. *J. Mol. Biol. 187*, 131−135.
(60) Margoshes, M., and Vallee, B. L. (1957) A Cadmium Protein from Equine Kidney Cortex. *J. Am. Chem. Soc. 79*, 4813−4814.
(61) Kägi, J. H. R. (1991) Overview of metallothionein. *Methods Enzymol. 205*, 613−626.
(62) Henkel, G., and Krebs, B. (2004) Metallothioneins: zinc, cadmium, mercury, and copper thiolates and selenolates mimicking protein active site features–structural aspects and biological implications. *Chem. Rev. 104*, 801−824.
(63) Klaassen, C. D., Liu, J., and Diwan, B. A. (2009) Metallothionein protection of cadmium toxicity. *Toxicol. Appl. Pharmacol. 238*, 215−220.
(64) Duncan, K. E., Ngu, T. T., Chan, J., Salgado, M. T., Merrifield, M. E., and Stillman, M. J. (2006) Peptide folding, metal-binding mechanisms, and binding site structures in metallothioneins. *Exp. Biol. Med. 231*, 1488−1499.
(65) Bremner, I., and Young, B. W. (1976) Isolation of (copper, zinc-) thioneins from pig liver. *Biochem. J. 155*, 631−635.
(66) Capdevila, M., Bofill, R., Palacios, O., and Atrian, S. (2012) State-of-the-art of metallothioneins at the beginning of the 21stcentury. *Coord. Chem. Rev. 256*, 46−62.
(67) Pedrini-Martha, V., Schnegg, R., Baurand, P. E., deVaufleury, A., and Dallinger, R. (2017) The physiological role and toxicological significance of the non-metal-selective cadmium/copper-metallothionein isoform differ between embryonic and adult helicid snails. *Comp. Biochem. Physiol., Part C: Toxicol. Pharmacol. 199*, 38−47.
(68) Pedrini-Martha, V., Niederwanger, M., Kopp, R., Schnegg, R., and Dallinger, R. (2016) Physiological, Diurnal and Stress-Related Variability of Cadmium-Metallothionein Gene Expression in Land Snails. *PLoS One 11*, e0150442.
(69) Irving, H., and Williams, R. J. P. (1953) The stability of transition-metal complexes. *J. Chem. Soc.*, 3192−3210.
(70) Vašák, M., and Bogumil, R. (1997) Diversity of Cluster Structures in Mammalian Metallothionein: Interplay between Metal Ions and Polypeptide Chain. In *Cytotoxic, Mutagenic and Carcinogenic Potential of Heavy Metals Related to Human Environment* (Hadjiliadis, N. D., Ed.) pp 195−215, Kluwer.
(71) Neuhaus, D., Wagner, G., Vašák, M., Kägi, J. H. R., and Wüthrich, K. (1984) ^{113}Cd-^{1}H spin-spin couplings in homonuclear ^{1}H correlated spectroscopy of metallothionein. Identification of the cysteine ^{1}H spin systems. *Eur. J. Biochem. 143*, 659−667.
(72) Zerbe, O., Pountney, D. L., von Philipsborn, W., and Vašák, M. (1994) Vicinal ^{113}Cd,^{1}Hβ-Cysteine Coupling in Cd-Substituted Metalloprotein Follows a Karplus-Type Dependence. *J. Am. Chem. Soc. 116*, 377−378.
(73) Bertini, I., Hartmann, H. J., Klein, T., Liu, G., Luchinat, C., and Weser, U. (2000) High resolution solution structure of the protein part of Cu_7 metallothionein. *Eur. J. Biochem. 267*, 1008−1018.
(74) Cobine, P. A., McKay, R. T., Zangger, K., Dameron, C. T., and Armitage, I. M. (2004) Solution structure of Cu_6 metallothionein from the fungus Neurospora crassa. *Eur. J. Biochem. 271*, 4213−4221.
(75) Schultze, P., Wörgötter, E., Braun, W., Wagner, G., Vašák, M., Kägi, J. H. R., and Wüthrich, K. (1988) Conformation of [Cd_7]-metallothionein-2 from rat liver in aqueous solution determined by nuclear magnetic resonance spectroscopy. *J. Mol. Biol. 203*, 251−268.

DOI: 10.1021/acs.biochem.9b00830
Biochemistry 2019, 58, 4570−4581